

# Measurement of the $e^+e^- \rightarrow K_S K_L$ cross section near the $\phi(1020)$ resonance with the SND detector

M. N. Achasov,<sup>1,2</sup> A. Yu. Barnyakov,<sup>1,2</sup> E. V. Bedarev,<sup>1,2</sup> K. I. Beloborodov,<sup>1,2</sup> A. V. Berdyugin,<sup>1,2</sup>  
A. G. Bogdanchikov,<sup>1</sup> A. A. Botov,<sup>1</sup> D. E. Chistyakov,<sup>1,2</sup> T. V. Dimova,<sup>1,2</sup> V. P. Druzhinin,<sup>1,2,\*</sup>  
L. V. Kardapoltsev,<sup>1,2</sup> A. S. Kasaev,<sup>1</sup> A. A. Kattsin,<sup>1</sup> A. G. Kharlamov,<sup>1,2</sup> I. A. Koop,<sup>1,2</sup>  
A. A. Korol,<sup>1,2</sup> D. P. Kovrizhin,<sup>1</sup> A. S. Kupich,<sup>1,2</sup> A. P. Kryukov,<sup>1</sup> N. A. Melnikova,<sup>1,2</sup>  
N. Yu. Muchnoi,<sup>1,2</sup> A. E. Obrazovsky,<sup>1</sup> E. V. Pakhtusova,<sup>1</sup> K. V. Pugachev,<sup>1,2</sup> S. A. Rastigeev,<sup>1</sup>  
Yu. A. Rogovsky,<sup>1,2</sup> A. I. Senchenko,<sup>1</sup> S. I. Serednyakov,<sup>1,2</sup> Yu. M. Shatunov,<sup>1</sup> S. P. Sherstyuk,<sup>1,2</sup>  
D. A. Shtol,<sup>1</sup> Z. K. Silagadze,<sup>1,2</sup> I. K. Surin,<sup>1</sup> Yu. V. Usov,<sup>1</sup> V. N. Zhabin,<sup>1,2</sup> and Yu. M. Zharinov<sup>1</sup>  
(SND Collaboration)

<sup>1</sup>*Budker Institute of Nuclear Physics, SB RAS, Novosibirsk, 630090, Russia*

<sup>2</sup>*Novosibirsk State University, Novosibirsk, 630090, Russia*

The cross section for the  $e^+e^- \rightarrow K_S K_L$  process is measured in the center-of-mass energy range from 1000 MeV to 1100 MeV in the experiment with the SND detector at the VEPP-2000  $e^+e^-$  collider. The measurement is carried out in the  $K_S \rightarrow 2\pi^0$  decay mode. Data with an integrated luminosity of  $20 \text{ pb}^{-1}$  recorded in 2018 at 18 energy points are used in the analysis. The systematic uncertainty in the measured cross section at the maximum of the  $\phi$  resonance is 0.9%. The mass, width of the  $\phi$  meson, and the product of the branching fractions  $B(\phi \rightarrow K_S K_L)B(\phi \rightarrow e^+e^-)$  are determined from the fit to the cross-section energy dependence.

## I. INTRODUCTION

This work is devoted to the measurement of the cross section for the  $e^+e^- \rightarrow K_S K_L$  process in the center-of-mass energy region  $E = \sqrt{s} = 1000\text{--}1100$  MeV with the SND detector at the VEPP-2000 collider. In this region, the dominant contribution to the cross section comes from the  $\phi(1020)$  resonance. The non-resonant contribution coming from the  $\rho$  and  $\omega$  tails and excited vector resonances is less than 0.1% at the resonance maximum [1]. Therefore, the  $e^+e^- \rightarrow K_S K_L$  process is the best for determining the mass and width of the  $\phi(1020)$  resonance. In particular, the values of these parameters obtained in this work are planned to be used in future SND analyses for the processes  $e^+e^- \rightarrow \pi^+\pi^-\pi^0$  and  $e^+e^- \rightarrow \pi^0\gamma$ , in which the effects of interference with non-resonant amplitudes are significantly larger than in the process  $e^+e^- \rightarrow K_S K_L$ .

The energy region under study is near the threshold of the  $e^+e^- \rightarrow K_S K_L$  reaction. Therefore, its cross section is sensitive to the effects of final-state interaction (FSI). The FSI contribution increases as the threshold is approached. For example, at  $E = 1000$  MeV, the cross section due to FSI is expected to increase by 16% [2]. In this analysis, we will fit the measured  $e^+e^- \rightarrow K_S K_L$  cross section taking into account the contribution of the final-state interaction.

The main task of experiments at the VEPP-2000  $e^+e^-$  collider is the precision measurement of the total hadronic cross section, needed, in particular, to calculate the hadron contribution to the anomalous magnetic moment of the muon  $a_\mu$ . To reach the accuracy of the  $a_\mu$  cal-

ulation equal to the expected accuracy of the Fermilab experiment (0.14 ppm) [3], the cross section of the dominant process  $e^+e^- \rightarrow \pi^+\pi^-$  must be measured with an accuracy of 0.2% (see, for example, [4]). For the process  $e^+e^- \rightarrow K_S K_L$  near the  $\phi(1020)$  resonance, the required accuracy is about 1%.

In the energy range under study, the most accurate measurements of the  $e^+e^- \rightarrow K_S K_L$  cross sections were carried out in the SND [5] and CMD-2 [6] experiments at the VEPP-2M collider and in the CMD-3 [1] experiment at the VEPP-2000 collider. The systematic errors in the cross section in these experiments are 3.2%, 1.7%, and 1.8%, respectively. In this analysis we achieve a systematic uncertainty of 0.9%.

## II. DETECTOR AND EXPERIMENT

The Spherical Neutral Detector (SND) is a general-purpose non-magnetic detector collecting data at the VEPP-2000  $e^+e^-$  collider [7]. A detailed description of detector subsystems can be found in Refs. [8–11]. The parameters of charged particles are measured using a nine-layer drift chamber and a proportional chamber with cathode-strip readout located in a common gas volume. The solid angle of the tracking system is 94% of  $4\pi$ . Its azimuthal and polar angle resolutions are  $0.45^\circ$  and  $0.8^\circ$ , respectively. A system of aerogel threshold Cherenkov counters is located around the tracking system. The most important part of the detector for the current analysis is the three-layer spherical electromagnetic calorimeter consisting of 1640 NaI(Tl) crystals. The solid angle of the calorimeter is 95% of  $4\pi$ . Its energy resolution for photons is  $\sigma_{E_\gamma}/E_\gamma = 4.2\%/\sqrt[4]{E_\gamma(\text{GeV})}$ , and the angular resolution is about  $1.5^\circ$ . The calorimeter is surrounded

\* druzhinin@inp.nsk.su

by a 10 cm thick iron absorber, behind which there is a muon system consisting of proportional tubes and scintillation counters.

The process  $e^+e^- \rightarrow K_S K_L$  is analyzed in the decay mode  $K_S \rightarrow \pi^0 \pi^0$ . At  $E = 1020$  MeV the  $K_S$  meson has a decay length of about 6 mm and decays in 96% of cases inside the beam pipe with a radius of 20 mm. The  $K_L$  meson, which has a lifetime 570 times longer, is absorbed in most events due to nuclear interaction in the detector calorimeter. In this case, it is detected as one or more photons. In 27% of events,  $K_L$  crosses the calorimeter without interaction. Thus, most events of the process under study fall into the class of events with four or more detected photons. The  $e^+e^- \rightarrow K_S K_L$  process is the dominant multiphoton process in the  $\phi(1020)$  resonance region. The only source of the resonant background is the process  $e^+e^- \rightarrow \eta\gamma \rightarrow 3\pi^0\gamma$ , which has a cross section 25 times smaller at the resonance maximum.

The Monte Carlo generators of signal and background events take into account radiative corrections [13]. The angular distribution of the hard photon emitted from the initial state is generated according to Ref. [14]. The interactions of particles produced in  $e^+e^-$  annihilation with the detector material are simulated using the GEANT4 software package [15]. The analysis of processes with the  $K_L$  meson in the final state depends critically on the correctness of its nuclear interaction simulation. The nuclear interaction cross section in GEANT4 was modified according to Ref. [16] and then reduced by 5% to correctly reproduce the fraction of events, in which the  $K_L$  meson crossed the calorimeter without interaction.

The simulation takes into account variations of experimental conditions during data taking, in particular, dead detector channels and beam-induced background. The beam background leads to the appearance of spurious photons and charged particles in detected events. To take this effect into account, the simulation uses special background events recorded during data taking with a random trigger, which are superimposed on simulated events.

The analysis uses data recorded by SND in 2018 in the energy range  $E = 1000$ – $1100$  MeV. The integrated luminosity accumulated at 18 energy points is about  $20 \text{ pb}^{-1}$ . To study the background, data recorded below the threshold of the  $e^+e^- \rightarrow K_S K_L$  reaction are also used, in particular, about  $0.7 \text{ pb}^{-1}$  at energies of 984 and 990 MeV.

During data taking, the average beam energy and the energy spread were measured by a special system using the Compton back-scattering of laser photons on the electron beam [12]. The systematic uncertainty of the beam energy determination by this method was estimated in Ref. [12] by comparison with the energy measurement by the resonance depolarization method at  $E_b = 510$  and 460 MeV, where  $E_b$  is the beam energy. It is  $\Delta E_b/E_b = 6 \times 10^{-5}$  or about 60 keV for the center-of-mass energy  $E = 2E_b = 1000$  MeV. This uncertainty characterizes the possible shift of the energy scale. The

TABLE I. The center-of-mass energy ( $E$ ), center-of-mass energy spread ( $\sigma_E$ ) and integrated luminosity ( $IL$ ). For luminosity, the first error is statistical, the second is systematic.

| $E$ , GeV            | $\sigma_E$ , keV | $IL$ , $\text{pb}^{-1}$   |
|----------------------|------------------|---------------------------|
| $1000.280 \pm 0.086$ | $249 \pm 58$     | $601.2 \pm 2.3 \pm 11.0$  |
| $1001.908 \pm 0.030$ | $335 \pm 8$      | $634.2 \pm 2.5 \pm 2.7$   |
| $1005.986 \pm 0.022$ | $356 \pm 11$     | $1680.2 \pm 4.1 \pm 7.3$  |
| $1009.596 \pm 0.016$ | $352 \pm 13$     | $725.7 \pm 2.7 \pm 4.3$   |
| $1015.736 \pm 0.018$ | $385 \pm 13$     | $627.9 \pm 2.5 \pm 4.2$   |
| $1016.800 \pm 0.034$ | $351 \pm 20$     | $1650.1 \pm 4.4 \pm 8.4$  |
| $1017.914 \pm 0.032$ | $352 \pm 18$     | $1257.5 \pm 3.7 \pm 7.4$  |
| $1019.078 \pm 0.016$ | $373 \pm 8$      | $2454.7 \pm 5.7 \pm 14.5$ |
| $1019.940 \pm 0.016$ | $397 \pm 11$     | $2637.2 \pm 6.0 \pm 13.4$ |
| $1020.908 \pm 0.014$ | $396 \pm 13$     | $1426.6 \pm 4.1 \pm 6.2$  |
| $1022.092 \pm 0.014$ | $363 \pm 11$     | $1232.5 \pm 3.7 \pm 7.3$  |
| $1022.932 \pm 0.028$ | $369 \pm 23$     | $820.0 \pm 2.9 \pm 4.2$   |
| $1027.736 \pm 0.024$ | $373 \pm 17$     | $659.2 \pm 2.6 \pm 5.0$   |
| $1033.816 \pm 0.036$ | $366 \pm 16$     | $537.4 \pm 2.3 \pm 4.1$   |
| $1039.788 \pm 0.036$ | $423 \pm 23$     | $585.8 \pm 2.5 \pm 9.0$   |
| $1049.804 \pm 0.046$ | $427 \pm 23$     | $634.2 \pm 2.6 \pm 5.4$   |
| $1060.016 \pm 0.032$ | $393 \pm 35$     | $607.1 \pm 2.5 \pm 3.6$   |
| $1100.020 \pm 0.046$ | $447 \pm 13$     | $1426.1 \pm 4.4 \pm 6.2$  |

relative shift between points of the energy scan is smaller. Energy measurements performed at a given energy point are averaged with weights proportional to the integrated luminosity. The obtained energy values and their errors are listed in Table I. The error of the measured energy includes the statistical error and the uncertainty due to the beam energy drift during data taking. Also, the values of the average energy spread  $\sigma_E$  and their statistical errors are listed in Table I. The systematic error of  $\sigma_E$  does not exceed a fractional error of 5%.

### III. LUMINOSITY MEASUREMENT

The process  $e^+e^- \rightarrow \gamma\gamma$  is used for luminosity measurement. Like the process under study, it does not contain charged particles in the final state. Therefore, some uncertainties in the measurement of the  $e^+e^- \rightarrow K_S K_L$  cross section associated with the hardware event selection and beam-induced background are canceled out as a result of normalization to the luminosity. We select events without charged tracks and with at least two photons. The energies of the two most energetic photons in the event ( $E_{1,2}$ ) must be greater than  $0.3E$ . The azimuthal ( $\varphi_{1,2}$ ) and polar ( $\theta_{1,2}$ ) angles of these photons must satisfy the following conditions:  $|\Delta\varphi| = ||\varphi_1 - \varphi_2| - 180^\circ| < 15^\circ$ ,  $|\Delta\theta| = |\theta_1 + \theta_2 - 180^\circ| < 25^\circ$  and  $\theta^* = (180^\circ - |\theta_1 - \theta_2|)/2 > 45^\circ$ . The latter condition limits the range of polar angles for photons. Unlike the angles  $\theta_{1,2}$ , the average polar angle of two photons  $\theta^*$  is practically insensitive to the position of the event vertex along the beam axis, which has a spread of  $\sigma_z \approx 3$  cm.

The detection efficiency and the cross section for the  $e^+e^- \rightarrow \gamma\gamma$  process are determined using the BabaYaga-

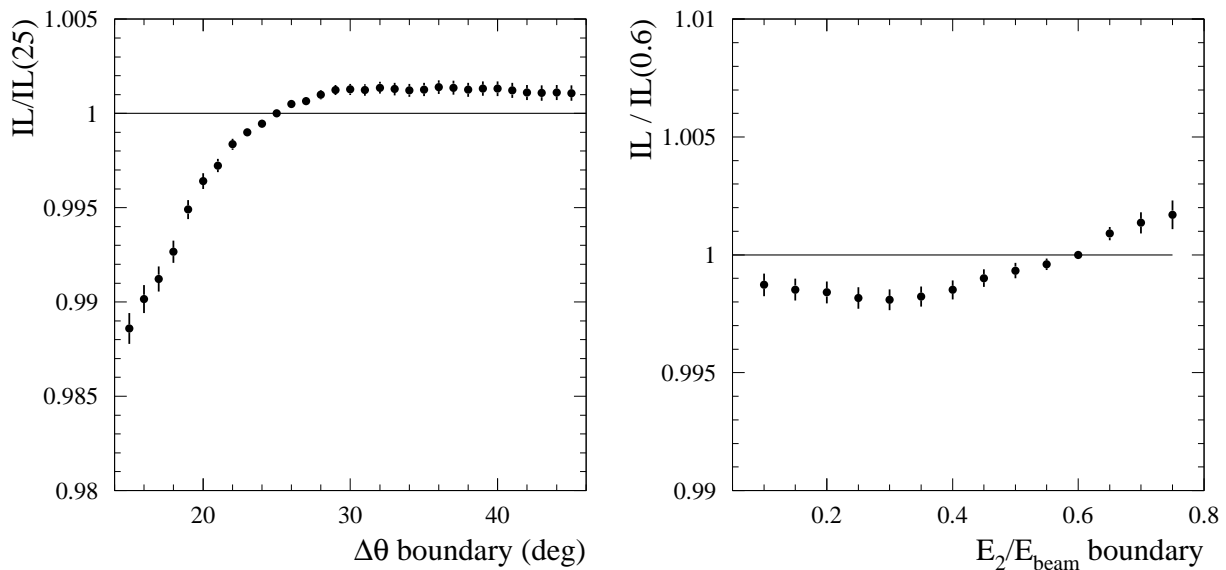


FIG. 1. The relative change of the measured integrated luminosity at  $E = 1019$  MeV as a function of the boundary on  $|\Delta\theta|$  (left) and the photon energy  $\min(E_1, E_2)$  (right).

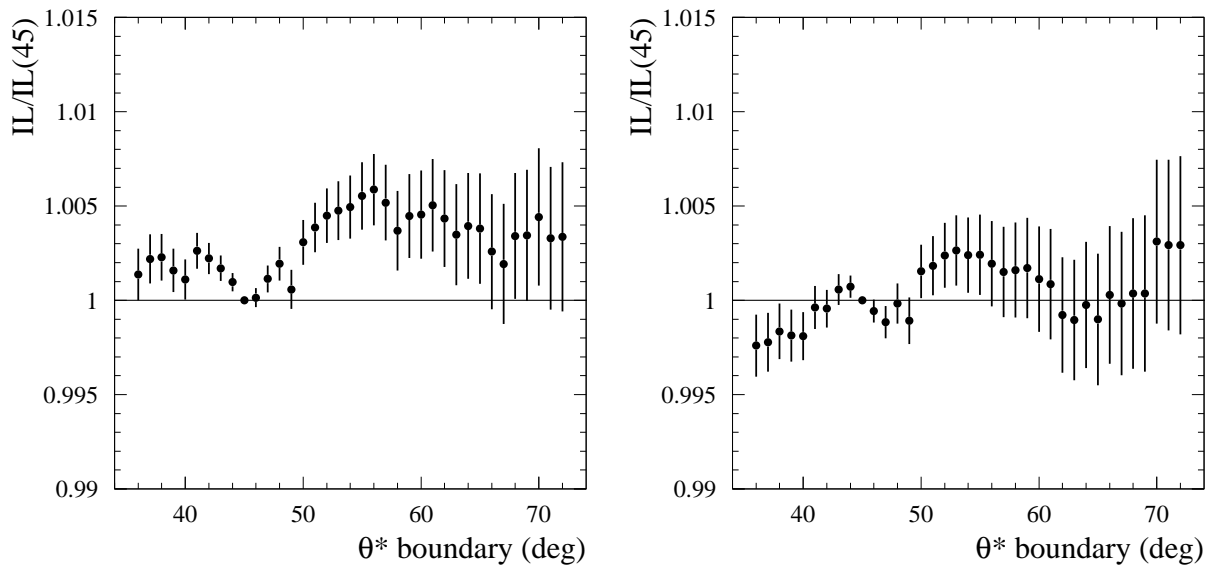


FIG. 2. The relative change of the measured integrated luminosity as a function of the boundary on  $\theta^*$  at  $E = 1019$  MeV (left) and  $1021$  MeV (right).

NLO Monte Carlo event generator [17]. To take into account the inaccuracy of the detector response simulation for photons, we determine corrections to the detection efficiency. To do this, the selection conditions described above are varied in turn over a wide range. Depending on the presence of background, the remaining conditions could be tightened. Figure 1 shows how the measured integrated luminosity at  $E = 1019$  MeV changes with varying the conditions on  $\Delta\theta$  and the en-

ergy of the second least energetic photon. It is seen that when the conditions on  $E_2$  and  $\Delta\theta$  are relaxed, the relative change in luminosity approaches a constant level of about  $-0.15\%$  for  $E_2$  and  $0.15\%$  for  $\Delta\theta$ . These values with errors of  $0.05\%$  are taken as corrections to the luminosity. The correction for the condition on  $\Delta\varphi$  is not needed. Figure 2 shows the relative changes in luminosity  $IL/IL(45^\circ)$  when varying the condition on  $\theta^*$  for  $E = 1019$  MeV and  $E = 1021$  MeV. In this case, no cor-

rection is introduced, and the variations of  $IL/IL(45^\circ)$  relative to unity are used to estimate the systematic uncertainty in the measured luminosity. It is equal to 0.5% at  $E = 1019$  MeV and 0.3% at  $E = 1021$  MeV. Similar studies are performed for all energy points.

Another efficiency correction arises from incorrect simulation of photon conversion in detector material before the drift chamber. The converted photon is usually reconstructed as a single charged particle. Such an event is rejected by the selection conditions. The conversion probability is measured using events of the process  $e^+e^- \rightarrow \pi^0\gamma$  at the maximum of the  $\omega(782)$  resonance, where this process has a large cross section and can be easily separated from background in the class of events with a single charged particle. The photon conversion probability in data is found to be greater than that in the simulation by  $(0.23 \pm 0.02)\% / \sin\theta_\gamma$ , where  $\theta_\gamma$  is the photon polar angle. For the process  $e^+e^- \rightarrow \gamma\gamma$  with the selection described above, the correction for photon conversion is  $(0.53 \pm 0.04)\%$ .

In the  $e^+e^- \rightarrow K_S K_L$  analysis (see Sec. VII), we introduce a correction for the presence of a charged track in the event. In  $e^+e^- \rightarrow \gamma\gamma$  events, the main source of extra charged tracks, in addition to conversion, is superimposing beam-induced background on the events of interest. To study it,  $e^+e^- \rightarrow \eta\gamma \rightarrow 3\gamma$  events with charged tracks originating outside the beam interaction region are analyzed. The probability of an extra track in the  $e^+e^- \rightarrow \eta\gamma$  event is found to be  $(0.4 \pm 0.2)\%$  larger in data than in simulation. This correction is applied to  $e^+e^- \rightarrow \gamma\gamma$  events.

The background sources for the  $e^+e^- \rightarrow \gamma\gamma$  events are cosmic rays and the  $e^+e^- \rightarrow \pi^0\gamma$  and  $e^+e^- \rightarrow \eta\gamma$  processes. Most of the cosmic events that pass the selection conditions for  $e^+e^- \rightarrow \gamma\gamma$  have a hit in the muon system ( $\mu_{\text{veto}} = 1$ ). For these events, we analyze the distribution of the arrival time of the calorimeter first-level-trigger signal relative to the beam collision time ( $\tau_{\text{FLT}}$ ). The distribution shown in Fig. 3 is fitted by the sum of the peaked distribution for  $e^+e^- \rightarrow \gamma\gamma$  events with  $\mu_{\text{veto}} = 0$  and a flat distribution for cosmic-ray events. The latter is obtained from data using the special selections described in Sec. V. As a result of the fit, the number of background cosmic-ray events is obtained. It is about 0.08% of the total number of  $e^+e^- \rightarrow \gamma\gamma$  events and is subtracted. The fraction of cosmic-ray events that do not fire the muon system ( $\mu_{\text{veto}} = 0$ ) is estimated using data recorded in 2018 at  $E = 548$  MeV. The events are processed assuming that  $E = 1020$  MeV. In this case, only background cosmic-ray events satisfy the  $e^+e^- \rightarrow \gamma\gamma$  selection criteria. The fraction of cosmic-ray events with  $\mu_{\text{veto}} = 0$  is found to be 20%. Thus, the unaccounted cosmic background does not exceed 0.02%. This number is used as a measure of the corresponding systematic uncertainty.

The processes  $e^+e^- \rightarrow \pi^0\gamma$  and  $e^+e^- \rightarrow \eta\gamma$  imitate  $e^+e^- \rightarrow \gamma\gamma$  events when the  $\pi^0$  ( $\eta$ ) meson decays along a direction close to the direction of its motion. The frac-

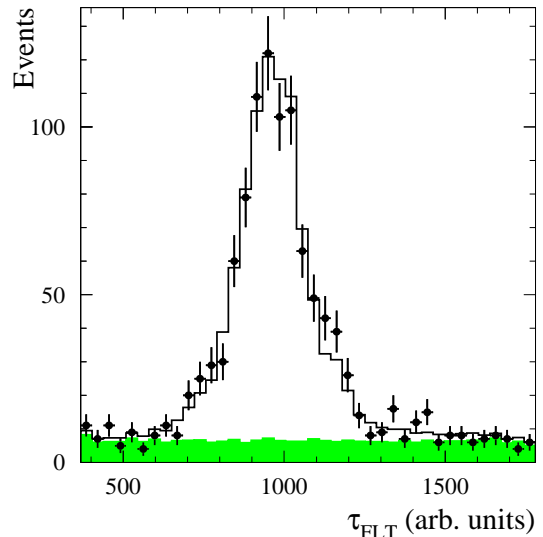


FIG. 3. The  $\tau_{\text{FLT}}$  distribution for  $e^+e^- \rightarrow \gamma\gamma$  candidate events with  $\mu_{\text{veto}} = 1$  at  $E = 1019$  MeV. The solid histogram shows the result of the fit by the sum of distributions for  $e^+e^- \rightarrow \gamma\gamma$  events and the cosmic-ray background. The shaded histogram represents the contribution of cosmic-ray events.

TABLE II. The contributions to the systematic uncertainty in the luminosity measurement ( $\Delta IL$ ) in the energy region 1017–1022 MeV from different sources.

| Source                                | $\Delta IL$ , % |
|---------------------------------------|-----------------|
| Condition $\theta^* > 45^\circ$       | 0.5             |
| Condition $ \Delta\theta  < 25^\circ$ | 0.05            |
| Condition $E_1, E_2 > 0.3E$           | 0.05            |
| Cosmic-ray background                 | 0.02            |
| Background from $\phi$ meson decays   | 0.2             |
| Photon conversion                     | 0.04            |
| Beam-induced charged tracks           | 0.2             |
| Theoretical uncertainty               | 0.1             |
| <b>Total</b>                          | <b>0.6</b>      |

tion of background events in the maximum of the  $\phi$  resonance determined using simulation is 3%. The ratio of  $e^+e^- \rightarrow \pi^0\gamma$  and  $e^+e^- \rightarrow \eta\gamma$  background events is close to 1:1. The fraction of background events in the class of events with exactly two photons is 0.3%. Therefore, the ratio of the numbers of events with  $N_\gamma > 2$  and  $N_\gamma = 2$  can be used to estimate the accuracy of the background simulation. Its energy dependence has a resonance component. Its value is reproduced by simulation with an accuracy of 5%. Thus, the systematic uncertainty associated with the resonance background from the processes  $e^+e^- \rightarrow \pi^0\gamma$  and  $e^+e^- \rightarrow \eta\gamma$  does not exceed 0.2%.

The integrated luminosity is determined as follows

$$IL = \frac{N_{\gamma\gamma} - N_{\text{csm}}}{\sigma_{\gamma\gamma} + \sigma_{\eta\gamma} + \sigma_{\pi^0\gamma}}, \quad (1)$$

where  $N_{\gamma\gamma}$  is the number of selected data events,  $N_{csm}$  is the measured cosmic ray background,  $\sigma_{\gamma\gamma}$ ,  $\sigma_{\eta\gamma}$ , and  $\sigma_{\pi^0\gamma}$  are the cross sections for the processes  $e^+e^- \rightarrow \gamma\gamma$ ,  $e^+e^- \rightarrow \eta\gamma$ , and  $e^+e^- \rightarrow \pi^0\gamma$ , respectively, calculated for the selection criteria described above using simulation. The distribution of the integrated luminosity over energy points is given in Table I with statistical and systematic errors. For the energy region 1017–1022 MeV, the systematic uncertainty does not exceed 0.6%. The contributions to the systematic uncertainty from different sources are listed in Table II.

#### IV. SELECTION OF $e^+e^- \rightarrow K_S K_L$ EVENTS

To measure the  $e^+e^- \rightarrow K_S K_L$  cross section near the threshold, the selection conditions must provide strong suppression of background events. Therefore, events are selected in which all four photons from the decay of  $\pi^0$  mesons ( $n_\gamma \geq 4$ ) are detected. It is required that there are no charged tracks in the drift chamber ( $n_{ch} = 0$ ). Then, a kinematic fit of events is performed with the constraints that two pairs of photons form  $\pi^0$  mesons, and two pions form a  $K_S$  meson. The quality of the fit is characterized by the parameter  $\chi_K^2$ . The distribution of this parameter for data events at  $E = 1019$  MeV is shown in Fig. 4 (left). It is compared with the simulated distribution. The shaded histogram shows the background contribution from the  $e^+e^- \rightarrow \eta\gamma$  process calculated using simulation. All other background sources at this energy give a negligible contribution. Also shown is the distribution for the cosmic-ray background obtained from events recorded below the  $e^+e^- \rightarrow K_S K_L$  threshold and selected with the additional requirement of a hit in the muon system ( $\mu veto = 1$ ).

The second parameter used for background suppression is the energy of the reconstructed  $K_S$  meson  $E_K$ . The  $2E_K/E$  distribution is shown in Fig. 4 (right). To suppress the background, the following conditions are imposed:

$$\chi_K^2 < 30, 2E_K/E < 1.05, \quad (2)$$

shown in Fig. 4 by arrows.

Events of the  $e^+e^- \rightarrow K_S K_L$  process can be divided into four classes listed in Table III. The main for analysis Class I contains events satisfying all the conditions described above. The detection efficiency of  $e^+e^- \rightarrow K_S K_L$  events in this class is 50% at  $E = 1019$  GeV. Events having  $n_\gamma \geq 4$  but not satisfying the conditions  $\chi_K^2 < 30$  and  $2E_K/E < 1.05$  fall into Class II. Class III with  $n_\gamma \leq 3$  mainly contains events, in which the  $K_L$  meson does not produce a signal in the calorimeter, and one of the photons from the  $\pi^0$  decays is lost. This class has a very high level of beam and cosmic-ray backgrounds. Class IV contains events with one or more charged tracks. The main causes of the charged track appearance in  $K_S K_L$  events are photon conversion in material before the drift chamber (4%),  $\pi^0 \rightarrow e^+e^-\gamma$  decay (2.3%),  $K_L$  meson decay

TABLE III. Four classes, into which  $e^+e^- \rightarrow K_S K_L$  events are divided by the selection conditions, and the fractions of events in these classes ( $f$ ) at  $E = 1019$  MeV calculated using simulation.

| Class | Selection conditions   | $f$ , % |
|-------|--|---------|
| IV    | $n_{ch} > 0$   | 15.4    |
| III   | $(n_{ch} = 0)$ AND $(n_\gamma < 4)$  | 7.1     |
| II    | $(n_{ch} = 0)$ AND $(n_\gamma \geq 4)$ AND NOT $[(\chi_K^2 < 30)$ AND $(2E_K/E < 1.05)]$ | 27.5    |
| I     | $(n_{ch} = 0)$ AND $(n_\gamma \geq 4)$ AND $(\chi_K^2 < 30)$ AND $(2E_K/E < 1.05)$       | 50.0    |

inside the drift chamber ( $\approx 4\%$ ), and beam background superimposing on  $K_S K_L$  events ( $\approx 5\%$ ).

To measure the  $e^+e^- \rightarrow K_S K_L$  cross section and the  $\phi$  meson parameters, the following strategy is used. The background is subtracted from data events selected with the standard conditions (Class I). Then the visible cross section is determined as

$$\sigma_{vis,i} = \frac{N_{K_S K_L,i}}{\varepsilon_i I L_i}, \quad (3)$$

where  $N_{K_S K_L,i}$ ,  $\varepsilon_i$  and  $I L_i$  are the number of selected  $K_S K_L$  events, the detection efficiency calculated using simulation, and the integrated luminosity, respectively, at the  $i$ -th energy point. The measured cross section is fitted with the vector meson dominance (VMD) model. At this stage, the resonance mass and width are determined, as well as the relative value of the nonresonant amplitude of the  $e^+e^- \rightarrow K_S K_L$  process.

The obtained model parameters are used in the analysis of Class II events. From the ratio of the number of  $K_S K_L$  events in Classes I and II in the data and simulation, the correction to the cross section  $\delta_{\chi^2}$  is calculated. Then, corrections are obtained for the loss of a photon  $\delta_\gamma$  and the presence of a charged track  $\delta_{ch}$  in the event, i.e., for the difference between data and simulation in the fraction of events falling into Class III and Class IV. The methods for determining the corrections  $\delta_{\chi^2}$ ,  $\delta_\gamma$ , and  $\delta_{ch}$  will be described in detail in Sec. VII. After introducing the corrections, we obtain the final result for the Born cross section of the process  $e^+e^- \rightarrow K_S K_L$  and the parameter  $B(\phi \rightarrow K_S K_L)B(\phi \rightarrow e^+e^-)$ .

#### V. BACKGROUND SUBTRACTION

The main sources of background in Class I are the processes  $e^+e^- \rightarrow \eta\gamma$  and  $e^+e^- \rightarrow \pi^0\pi^0\gamma$  and cosmic rays. Most cosmic-ray events that pass the selection conditions trigger the muon system ( $\mu veto = 1$ ). Figure 5 (left) shows the  $\tau_{FLT}$  distribution for events with  $\mu veto = 1$  at  $E = 1028$  MeV. To subtract the background, the distribution is fitted by the sum of a peaked distribution of events  $e^+e^- \rightarrow K_S K_L$  and a flat distribution for cosmic rays. The first distribution is obtained using events

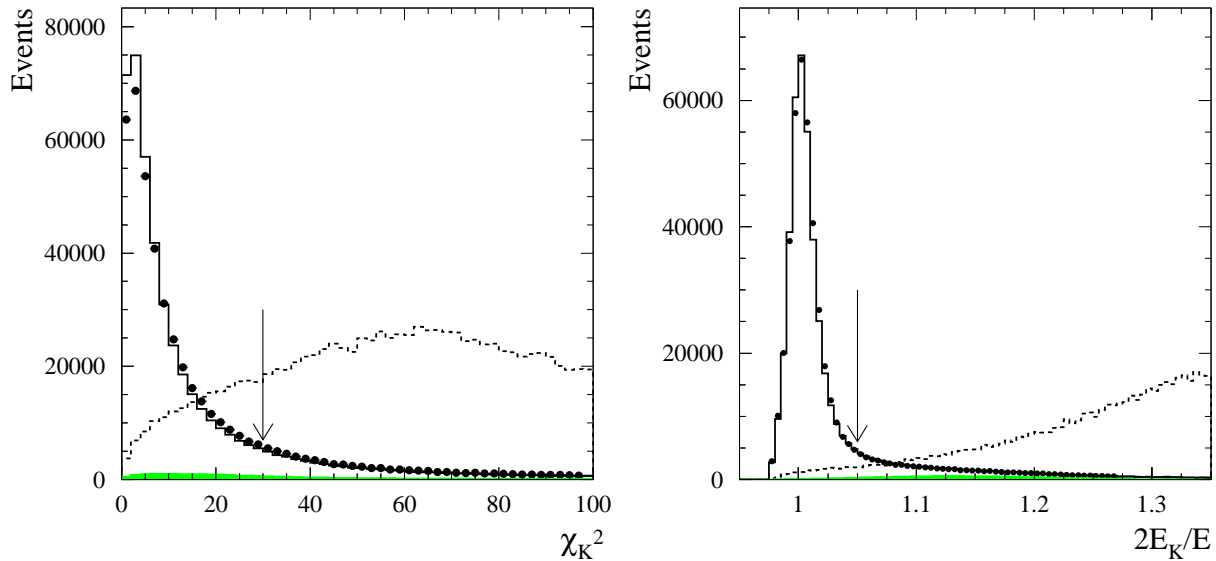


FIG. 4. The distributions of  $\chi_K^2$  (left) and  $2E_K/E$  (right) for data events (points with error bars) and simulations (solid histogram) at  $E = 1019$  GeV. The distributions are normalized to area. The shaded histogram represents the  $e^+e^- \rightarrow \eta\gamma$  background calculated using simulation. The dashed histogram shows the shape of the distribution for the cosmic-ray background. The arrows indicate the boundaries of the selection conditions.

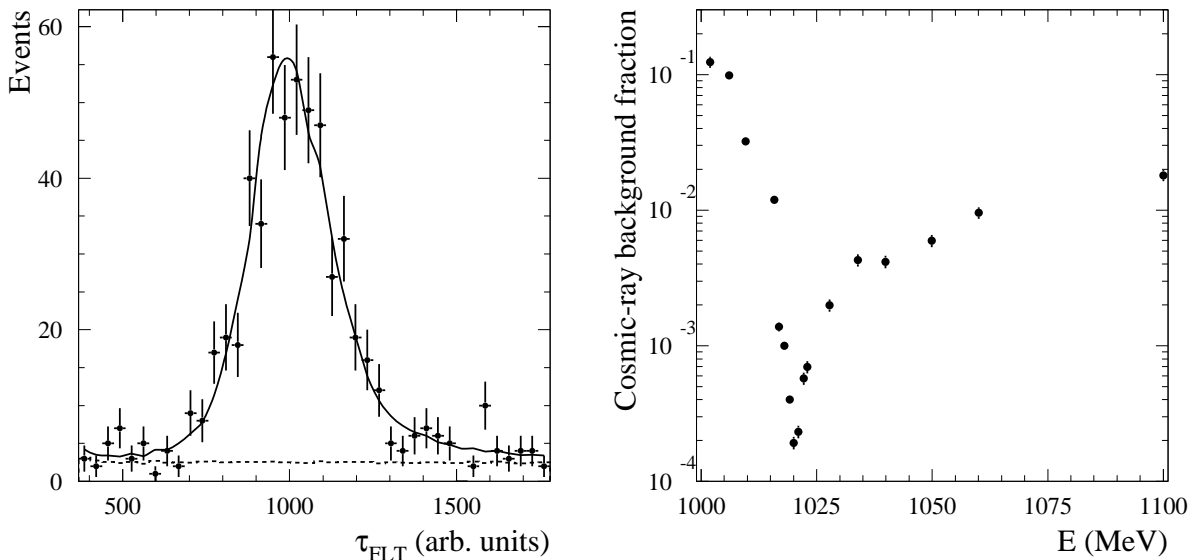


FIG. 5. Left panel: The  $\tau_{\text{FLT}}$  distribution for data events with  $\mu_{\text{veto}} = 1$  at  $E = 1028$  MeV. The solid curve represents the result of the fit to this distribution with the sum of signal and cosmic-ray background. Right panel: The fraction of cosmic-ray background in Class I.

with  $\mu_{\text{veto}} = 0$  at  $E = 1019$  MeV, and the second one is obtained using Class II events with  $\mu_{\text{veto}} = 1$  and  $30 < \chi_K^2 < 100$ , recorded below the  $e^+e^- \rightarrow K_S K_L$  threshold at  $E = 910$ – $930$  MeV. At  $E = 1000$  MeV, where the signal from  $e^+e^- \rightarrow K_S K_L$  events is not observed in the  $\tau_{\text{FLT}}$  spectrum due to the relatively high cosmic background level, events with  $\mu_{\text{veto}} = 1$  are re-

jected. The detection efficiency at this energy point is corrected accordingly. It should be noted that the muon system response for  $K_S K_L$  events is simulated incorrectly. At  $E > 1010$  MeV, the fraction of events with  $\mu_{\text{veto}} = 1$  is about 4% in the data and 6.5% in the simulation. At  $E \leq 1010$ , this fraction decreases to 5% in simulation. In data, its average value in the energy re-

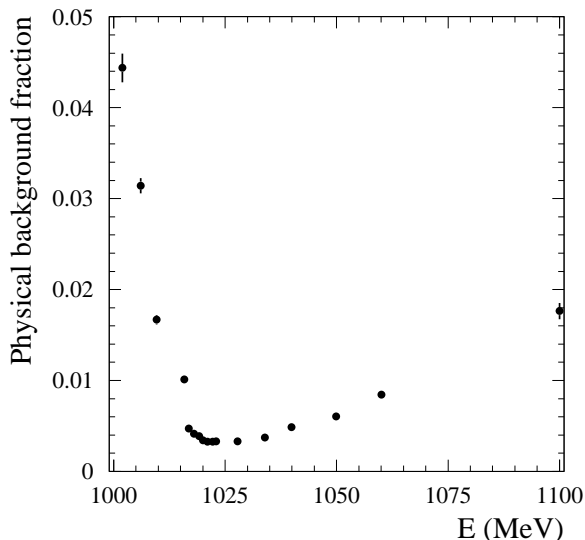


FIG. 6. The fraction of the  $e^+e^- \rightarrow \eta\gamma$  and  $e^+e^- \rightarrow \pi^0\pi^0\gamma$  background in Class I.

gion  $E = 1002\text{--}1010$  MeV is  $(4.1 \pm 0.6)\%$ . Therefore, for the point  $E = 1000$  MeV, we increase the detection efficiency by 1% and introduce an additional systematic uncertainty also equal to 1%.

In Class I with  $\mu\text{veto} = 0$ , the cosmic-ray background is determined using data with  $E = 910\text{--}930$  MeV. For these data, the  $\tau_{\text{FLT}}$  distribution is fitted, and the number of cosmic-ray events is determined. The expected background at the  $i$ th energy point is calculated as

$$N_{\text{cosm},i} = N_{\text{cosm},i}^0 \frac{t_i}{t_0}, \quad (4)$$

where  $t_i$  and  $t_0$  are the data taking times at the energy point  $i$  and at  $E = 910\text{--}930$  MeV ( $t_0 = 284000$  s,  $t_i \lesssim 100000$  s), and  $N_{\text{cosm},i}^0$  is the number of cosmic-ray events at  $E = 910\text{--}930$  MeV, obtained from the fit to the  $\tau_{\text{FLT}}$  distribution. Due to the condition  $2E_K/E_i < 1.05$ , the value of  $N_{\text{cosm},i}^0$  increases by a factor of 1.6 when  $E_i$  changes from 1000 to 1100 MeV. At the energy points  $E = 1000, 1001, 1003$  MeV, where the cross section of the process  $e^+e^- \rightarrow K_S K_L$  is small, the contribution of the cosmic-ray background for events with  $\mu\text{veto} = 0$  can be determined directly from the fit to the  $\tau_{\text{FLT}}$  distribution and then compared with Eq. (4). Their average ratio  $0.8 \pm 0.2$  agrees with unity. The difference of the ratio from unity by 20% is used as an estimate of the systematic uncertainty in determining the cosmic-ray background. The fraction of the beam background in Class I, shown in Fig. 5 (right), varies from 12% at  $E = 1000$  MeV to  $2 \times 10^{-4}$  at the maximum of the  $\phi$  resonance and then to 2% at  $E = 1100$  MeV.

The background from the processes  $e^+e^- \rightarrow \eta\gamma$  and  $e^+e^- \rightarrow \pi^0\pi^0\gamma$  is calculated using simulation. The  $e^+e^- \rightarrow \eta\gamma$  cross section in the event generator is cor-

rected using data as described in Sec. VII. To calculate the  $e^+e^- \rightarrow \pi^0\pi^0\gamma$  cross section, the approximation from Ref. [18] is used. The energy dependence of the fraction of background events in class I is shown in Fig. 6. The dominant contribution to the background comes from the process  $e^+e^- \rightarrow \eta\gamma$ . The accuracy of the background calculation is estimated using events from the sideband  $30 < \chi_K^2 < 100$ , where the  $e^+e^- \rightarrow \eta\gamma$  contribution can be measured as described in Sec. VII. It is better than 5%. The background level changes from 4.4% at  $E = 1000$  MeV to  $3 \times 10^{-3}$  at the maximum of the  $\phi$  resonance and then to 1.8% at  $E = 1100$  MeV.

Data collected near the  $e^+e^- \rightarrow K_S K_L$  threshold are most sensitive to the background level. For example, at  $E = 1000$  MeV, the number of selected  $K_S K_L$  events is  $N_{K_S K_L} = 128 \pm 16$  at  $IL = 0.60 \text{ pb}^{-1}$ . And at two points with  $E = 984$  MeV and 990 MeV, which are below the threshold, the number of selected events before background subtraction is 24, and after  $N_{K_S K_L} = 4 \pm 8$  at  $IL = 0.67 \text{ pb}^{-1}$ . The data below the threshold confirm the correctness of the background subtraction procedure.

The numbers of events in Class I after background subtraction are listed in Table IV. The first error is statistical, the second is systematic, related to the uncertainty in background subtraction.

## VI. FITTING THE MEASURED VISIBLE $e^+e^- \rightarrow K_S K_L$ CROSS SECTION.

Data on the visible cross section  $\sigma_{\text{vis},i}$  obtained using Eq. (3) are fitted by the following expression

$$\begin{aligned} \sigma_{\text{vis}}(E) &= \int_0^{x_{\text{max}}} F(E, x) \sigma(E\sqrt{1-x}) dx \\ &= \sigma(E)(1 + \delta(E)), \end{aligned} \quad (5)$$

where  $x = 2E_\gamma/E$ ,  $F(E, x)$  is a function describing the probability of emission of photons with energy  $E_\gamma$  from the initial state [13],  $\sigma(E)$  is the Born cross section for the process  $e^+e^- \rightarrow K_S K_L$ . The integration is carried out up to the kinematic limit  $x_{\text{max}} = 1 - 4m_{K^0}^2/E^2$ . To take into account the beam energy spread, it is necessary to perform a convolution of the cross section (5) with a Gaussian function describing the energy distribution of events. Since the energy spread is much smaller than the width of the  $\phi$  resonance, we use an approximate formula instead of convolution:

$$\begin{aligned} \sigma_{\text{vis}}(E) &\Rightarrow \sigma_{\text{vis}}(E) + \frac{1}{2} \frac{d^2 \sigma_{\text{vis}}(E)}{dE^2} \sigma_E^2 \\ &= \sigma_{\text{vis}}(E)(1 + \delta_E(E)) \end{aligned} \quad (6)$$

Near the  $\phi$  resonance the uncertainty in the collider energy listed in Table I effectively increases the uncertainty in the measured visible cross section. In fitting the cross-section energy dependence, the following term

TABLE IV. The center-of-mass energy ( $E$ ), detection efficiency ( $\varepsilon$ ), number of selected events ( $N_{K_S K_L}$ ), radiative correction ( $1 + \delta$ ), correction for the energy spread ( $1 + \delta_E$ ), Born cross section for the process  $e^+e^- \rightarrow K_S K_L$  ( $\sigma$ ). The first error in the number of events and cross section is statistical, the second is systematic.

| $E$ , GeV | $\varepsilon$ | $N_{K_S K_L}$           | $1 + \delta$ | $1 + \delta_E$ | $\sigma$ , nb              |
|-----------|---------------|-------------------------|--------------|----------------|----------------------------|
| 1000.280  | 0.129         | $128 \pm 16 \pm 1$      | 0.710        | 1.003          | $2.31 \pm 0.28 \pm 0.05$   |
| 1001.908  | 0.142         | $258 \pm 19 \pm 5$      | 0.720        | 1.005          | $3.96 \pm 0.29 \pm 0.08$   |
| 1005.986  | 0.143         | $2085 \pm 49 \pm 14$    | 0.733        | 1.004          | $11.76 \pm 0.29 \pm 0.13$  |
| 1009.596  | 0.145         | $2513 \pm 58 \pm 6$     | 0.734        | 1.006          | $32.28 \pm 0.79 \pm 0.31$  |
| 1015.736  | 0.150         | $20110 \pm 170 \pm 10$  | 0.715        | 1.021          | $293.02 \pm 2.9 \pm 2.9$   |
| 1016.800  | 0.151         | $91750 \pm 320 \pm 30$  | 0.709        | 1.019          | $511.18 \pm 2.3 \pm 4.6$   |
| 1017.914  | 0.150         | $119590 \pm 360 \pm 30$ | 0.707        | 1.008          | $892.92 \pm 4.0 \pm 8.3$   |
| 1019.078  | 0.149         | $348570 \pm 620 \pm 60$ | 0.721        | 0.973          | $1354.54 \pm 4.1 \pm 12.7$ |
| 1019.940  | 0.148         | $373190 \pm 640 \pm 70$ | 0.755        | 0.977          | $1297.56 \pm 3.8 \pm 11.5$ |
| 1020.908  | 0.148         | $157170 \pm 410 \pm 30$ | 0.812        | 1.004          | $916.45 \pm 3.8 \pm 7.7$   |
| 1022.092  | 0.151         | $92160 \pm 320 \pm 20$  | 0.891        | 1.010          | $550.02 \pm 2.6 \pm 5.1$   |
| 1022.932  | 0.151         | $47730 \pm 230 \pm 10$  | 0.947        | 1.009          | $404.02 \pm 2.5 \pm 3.6$   |
| 1027.736  | 0.152         | $14050 \pm 120 \pm 10$  | 1.218        | 1.003          | $114.53 \pm 1.4 \pm 1.2$   |
| 1033.816  | 0.153         | $5795 \pm 80 \pm 5$     | 1.459        | 1.001          | $48.14 \pm 1.1 \pm 0.5$    |
| 1039.788  | 0.154         | $4298 \pm 78 \pm 4$     | 1.625        | 1.001          | $29.39 \pm 0.95 \pm 0.52$  |
| 1049.804  | 0.151         | $2907 \pm 63 \pm 4$     | 1.815        | 1.000          | $16.71 \pm 0.71 \pm 0.22$  |
| 1060.016  | 0.156         | $2135 \pm 49 \pm 4$     | 1.941        | 1.000          | $11.64 \pm 0.55 \pm 0.17$  |
| 1100.020  | 0.156         | $2262 \pm 55 \pm 8$     | 2.154        | 1.000          | $4.73 \pm 0.26 \pm 0.14$   |

is quadratically added to the statistical error of  $\sigma_{\text{vis},i}$ :

$$\Delta E_i \frac{d\sigma_{\text{vis}}}{dE}(E_i), \quad (7)$$

where  $\Delta E_i$  is the uncertainty in the energy of  $i$ th point.

In the range  $E = 1016$ – $1023$  MeV, this additional uncertainty is comparable to or exceeds the statistical error.

To describe the Born cross section, the VMD model is used, which, in addition to the dominant amplitude of the  $\phi$  meson, includes the amplitudes of the  $\rho$  and  $\omega$  mesons and an amplitude that takes into account the contribution of the higher vector resonances [5]:

$$\begin{aligned} \sigma(E) = & \frac{12\pi}{E^3} \frac{\Gamma(\phi \rightarrow K_S K_L) P_K^3(E) m_\phi^2}{P_K^3(m_\phi)} \frac{m_\phi^2}{E^2} \left| \frac{\sqrt{m_\phi^3 \Gamma(\phi \rightarrow e^+ e^-)}}{D_\phi} e^{i\varphi_\phi} \right. \\ & \left. - k_{\text{SU3}} \left[ \frac{\sqrt{m_\omega^3 \Gamma(\omega \rightarrow e^+ e^-)}}{\sqrt{2} D_\omega} - \frac{\sqrt{m_\rho^3 \Gamma(\rho \rightarrow e^+ e^-)}}{\sqrt{2} D_\rho} \right] + A_0 \right|^2, \end{aligned} \quad (8)$$

with

$$P_K(E) = \sqrt{E^2/4 - m_{K_S}^2}, \quad D_V = m_V^2 - E^2 - iE\Gamma_V(E), \quad (9)$$

where  $m_V$ ,  $\Gamma(V \rightarrow e^+e^-)$ , and  $\Gamma_V(E)$  are the mass, partial width of the decay  $V \rightarrow e^+e^-$ , and the energy-dependent total width of the vector resonance  $V = \rho, \omega, \phi$ ,  $\Gamma(\phi \rightarrow K_S K_L)$  is the partial width of the decay  $\phi \rightarrow K_S K_L$ ,  $\varphi_\phi$  is the relative phase of the  $\phi$  meson amplitude,  $A_0$  is the amplitude describing the contributions of the higher vector resonances. When calculating the energy dependence of  $\Gamma_V(E)$ , decays with branching fractions greater than 1% are taken into account. In deriving the formula (8), the SU3 symmetry relationship between the coupling constants  $g_{\rho K_S K_L} = -g_{\omega K_S K_L} =$

$g_{\phi K_S K_L}/\sqrt{2}$  is used. The deviation of the coefficient  $k_{\text{SU3}}$  from unity characterizes the SU3 symmetry breaking.

In the fit, the phase  $\varphi_\phi$  is set to the value predicted by the quark model  $180^\circ$ , the coefficient  $k_{\text{SU3}} = 1$ . Since the energy region under study is located significantly below that of the excited resonances of the  $\rho$ ,  $\omega$ , and  $\phi$  families, and their widths decrease rapidly with decreasing energy, the amplitude  $A_0$  is assumed to be real. To take into account its small energy dependence, it is parametrized as  $A_0 = a_0/(1 - E^2/m_{\rho(1450)}^2)$ . The free parameters of the fit are the mass and width of the  $\phi$  meson,  $a_0$ , and



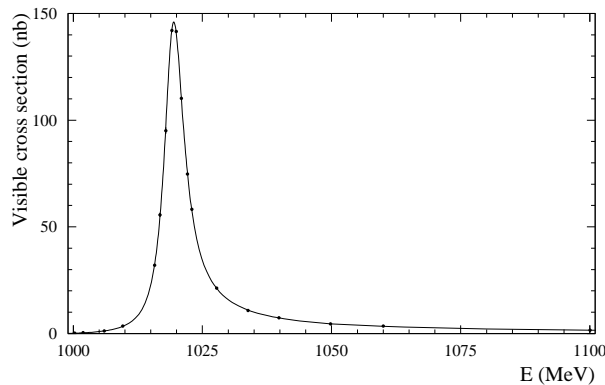


FIG. 7. The visible  $e^+e^- \rightarrow K_S K_L$  cross section for Class I events. The curve is the result of the fit described in the text.

the ratio  $R_\phi$  of the product  $B(\phi \rightarrow K_S K_L)B(\phi \rightarrow e^+e^-)$  obtained from our data to its Particle Data Group (PDG) value [19]. The remaining parameters of the model are fixed at their PDG values [19].

The result of the fit to the visible-cross-section data with Eq. (6) is shown in Fig. 7. The quality of the fit is not very good:  $\chi^2/\text{ndf} = 23.6/14$ . However, about 8 units of contribution to  $\chi^2$  come from 3 points near the  $e^+e^- \rightarrow K_S K_L$  threshold. Excluding these points from the fit leads to an acceptable value  $\chi^2/\text{ndf} = 14.2/11$ . In this case, the fit parameters change insignificantly. The deviation of the measured cross section from the VMD model near the threshold can be explained by the final state interaction. A model taking into account FSI will be discussed in Sec. VIII. The Born cross section parameters obtained from the VMD fit will be used in the next section to obtain corrections.

## VII. CORRECTIONS TO THE $e^+e^- \rightarrow K_S K_L$ CROSS SECTION

Figure 8 (left) shows the two-dimensional distribution of  $E_{\text{EMC}}/E$  versus  $P_{\text{EMC}}/E_{\text{EMC}}$  for data events with four or more photons that do not satisfy the condition on the parameters  $\chi_K^2$  and  $2E_K/E$  (Class II) at  $E = 1019$  MeV. Here  $E_{\text{EMC}}$  is the total energy deposition in the calorimeter, and  $P_{\text{EMC}}$  is the total event momentum calculated using the energy depositions in the calorimeter crystals. The solid broken line shows the boundary of a selection condition that significantly suppresses the beam-induced and cosmic-ray backgrounds. Beam background events usually have a small energy deposition in the calorimeter, and cosmic-ray background events have a large  $P_{\text{EMC}}/E_{\text{EMC}}$ . From the data recorded below the  $e^+e^- \rightarrow K_S K_L$  threshold, one can estimate that this selection condition suppresses the cosmic-ray background by about 10 times, and the beam background is suppressed by 20 times. At the same time, the num-

ber of  $K_S K_L$  events in Class II decreases insignificantly, by 3.6%. The accumulation of entries in Fig. 8 (left) with  $E_{\text{EMC}}/E$  near 0.9 and  $P_{\text{EMC}}/E_{\text{EMC}} < 0.2$  contains events of the processes  $e^+e^- \rightarrow \eta\gamma$  and  $e^+e^- \rightarrow \pi^0\pi^0\gamma$ , as well as the background from the electrodynamic processes  $e^+e^- \rightarrow 3\gamma, 4\gamma$ .

Subtraction of remaining cosmic-ray and physical backgrounds is performed as described in Sec. V. The background from the  $e^+e^- \rightarrow \eta\gamma$  process in Class II is about 12%. To ensure the required accuracy of subtraction of this background, we extract  $e^+e^- \rightarrow \eta\gamma$  events in the data and determine a scale factor to the number of events expected from the simulation. To determine the scale factor, we use events with  $N_\gamma > 4$ ,  $P_{\text{EMC}}/E_{\text{EMC}} < 0.22$  and  $E_{\text{EMC}}/E > 0.65 + P_{\text{EMC}}/E_{\text{EMC}}$ . The last two conditions are indicated by the dashed broken line in Fig. 8 (left). The fraction of  $e^+e^- \rightarrow \eta\gamma$  events in Class II satisfying these conditions is 74%. The energy distribution of the most energetic photon in an event for data events with  $E = 1019$  MeV is shown in Fig. 8 (right). It is fitted by the sum of the expected distributions for the simulated events of the processes  $e^+e^- \rightarrow \eta\gamma$ ,  $e^+e^- \rightarrow K_S K_L$ ,  $e^+e^- \rightarrow \pi^0\pi^0\gamma$  and  $e^+e^- \rightarrow 3\gamma, 4\gamma$ . The free fit parameters are the scale factors for the expected numbers of  $e^+e^- \rightarrow \eta\gamma$  and  $e^+e^- \rightarrow K_S K_L$  events. The result of the fit is shown in Fig. 8 (right). The scale factor for the  $e^+e^- \rightarrow \eta\gamma$  cross section is determined for all energy points. At the resonance maximum, its accuracy is 0.8%. Below 1012 MeV and above 1026 MeV, average values of the scale factors are used. Their accuracy is about 4%. Assuming that the fraction of the remaining  $e^+e^- \rightarrow \eta\gamma$  events is reproduced by the simulation with an accuracy of at least than 10%, we estimate that the number of background  $e^+e^- \rightarrow \eta\gamma$  events is predicted with an accuracy of at least than 3%.

The visible cross section for Class II events after background subtraction is fitted by the model described in the previous section with the parameters fixed at the values obtained in the fit to the cross section for Class I. The free fit parameters are the scale factor for the Born cross section and two parameters of the linear function describing the unaccounted background. The result of the fit is shown in Fig. 9 (left). It is seen that the level of the unaccounted background does not exceed 0.5% at the resonance maximum. From the fitted value of the scale factor, a correction to the cross section due to the difference between data and simulation in the fraction of  $K_S K_L$  events rejected by the conditions  $\chi_K^2 < 30$  and  $2E_K/E < 1.05$  is calculated. It is found to be  $\delta_{\chi^2} = 1.001 \pm 0.004$ . The correction uncertainty is mainly determined by the accuracy of  $e^+e^- \rightarrow \eta\gamma$  background subtraction.

The next correction accounts for the difference between data and simulation in the probability of the  $K_S K_L$  event falling into Class III with  $n_\gamma < 4$ . It is impossible to analyze events of this class directly due to the high level of beam and cosmic-ray backgrounds. Instead, we study

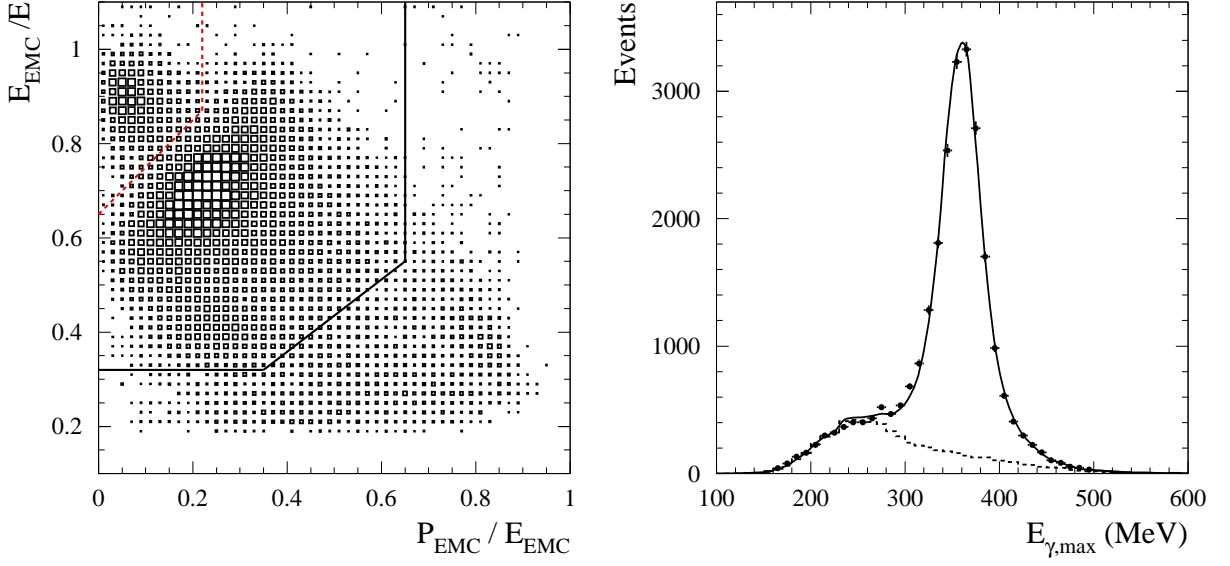


FIG. 8. Left panel: The distribution of  $E_{EMC}/E$  versus  $P_{EMC}/E_{EMC}$  for Class II data events. The solid broken line indicates the boundary of the background suppression condition. The dashed broken line indicates the the boundary of the selection condition for  $\eta\gamma$  events. Right panel: The energy distribution of the most energetic photon  $E_{\gamma,max}$  for data events at  $E = 1019$  MeV. The curve is the result of the fit by the sum of contributions from processes  $e^+e^- \rightarrow \eta\gamma$ ,  $e^+e^- \rightarrow K_S K_L$ ,  $e^+e^- \rightarrow \pi^0 \pi^0 \gamma$  and  $e^+e^- \rightarrow 3\gamma, 4\gamma$ . The dotted curve is the sum of contributions from all processes except  $e^+e^- \rightarrow \eta\gamma$ .

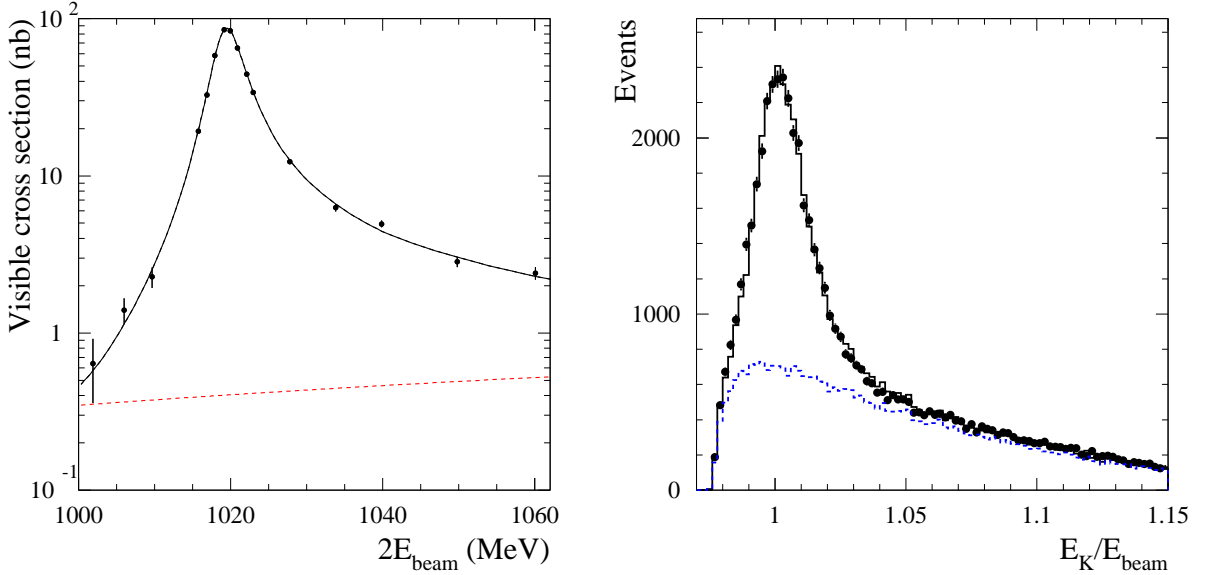


FIG. 9. Left panel: The visible cross section for events from Class II. The curve is the result of the fit described in the text. The dotted line shows the background contribution. Right panel: The  $2E_K/E$  distribution for events with one central charged track at  $E = 1019$  MeV. The solid histogram is the result of the fit by the sum of the simulated signal and background distributions. The dotted histogram is the background distribution.

events containing a well-identified  $K_L$  meson. The  $K_L$  candidate is a particle reconstructed as a single photon with an energy greater than  $0.3E$ , which has a transverse distribution of energy depositions in the calorimeter crystals unlikely for a photon shower. We compare the results

of the fits to the visible cross sections for events with the  $K_L$  candidate and three or four photons. In data, the fraction of events with three photons turn out to be approximately 13% larger than in simulation. The corresponding correction to the  $e^+e^- \rightarrow K_S K_L$  cross section

is  $\delta_\gamma = 1.012 \pm 0.003$ .

The last correction is related to  $e^+e^- \rightarrow K_S K_L$  events containing charged tracks (Class IV). When analyzing events with  $n_{\text{ch}} > 0$ , all clusters in the calorimeter are considered as photons. The presence of four or more photons and  $\chi_K^2 < 30$  are required. Events with two central charged tracks (12%), one central track (43%), and no central tracks (45%) are analyzed separately. A central charged track is a track originating from the beam interaction region. The fraction of events with  $n_{\text{ch}} > 0$  in each subclass is given in the parentheses. The background sources are the processes  $e^+e^- \rightarrow K^+K^-$ ,  $e^+e^- \rightarrow \pi^+\pi^-\pi^0$  and  $e^+e^- \rightarrow K_S K_L$  with the decay  $K_S \rightarrow \pi^+\pi^-$ . To suppress the background in the class with two central tracks, we additionally require the presence of the  $K_L$  candidate, as described in the previous paragraph. To subtract the background, we fit the  $2E_K/E$  distribution by the sum of the simulated signal and background distributions. The result of the fit for events with one central track at  $E = 1019$  MeV is shown in Fig. 9 (right). To estimate the systematic uncertainty associated with background subtraction, in the classes with zero and one central track, where the dominant background process is  $e^+e^- \rightarrow K^+K^-$ , we vary the condition on  $\chi_K^2$ . In the class with two central tracks, the distribution of the spatial angle between charged particles is additionally analyzed, from which information on the relative contributions of background processes is extracted. The correction is calculated from the difference between data and simulation in the ratio of  $K_S K_L$  events with  $n_{\text{ch}} > 1$  and  $n_{\text{ch}} = 0$ . The correction to the cross section is  $\delta_{\text{ch}} = 1.014 \pm 0.005$ . The correction uncertainty is determined by the accuracy of background shape simulation.

The total correction to the cross section is  $a_{\text{cor}} = 1.027 \pm 0.007$ . Technically, this correction is introduced into the detection efficiency determined from simulation. The corrected detection efficiency multiplied by  $B(K_S \rightarrow \pi^0\pi^0) = 0.3069 \pm 0.0005$  [19] is listed in Table IV. It is seen that the efficiency weakly depends on energy and is about 15%.

## VIII. RESULTS

The parameters of the model described in Sec. VI, obtained from the fit to the visible-cross-section data are listed in Table V. The second column represents the result of the fit to the cross section over all 18 energy points. As already mentioned, 8 units in  $\chi^2$  come from the first three points located near the threshold. The parameters obtained after removing these points from the fit are listed in the third column. It is natural to assume that the deviation of the measured cross section from the model near the threshold can be caused by the interaction of kaons in the final state. The effect of FSI is taken into account with the factor [2], by which the Born cross section (8) is multiplied. This factor is normalized

TABLE V. The parameters of the model described in Sec. VI (VMD), and the same model, but taking into account FSI (VMD+FSI). The number of energy points used in the fit is given in the parentheses after the model name. Only statistical errors of the parameters are quoted.

| Parameter             | VMD(18)            | VMD(15)            | VMD+FSI(18)        |
|-----------------------|--------------------|--------------------|--------------------|
| $R_\phi$              | $0.974 \pm 0.003$  | $0.975 \pm 0.003$  | $0.975 \pm 0.003$  |
| $\Delta m_\phi$ , MeV | $-0.018 \pm 0.010$ | $-0.018 \pm 0.010$ | $-0.002 \pm 0.010$ |
| $\Gamma_\phi$ , MeV   | $4.230 \pm 0.019$  | $4.212 \pm 0.020$  | $4.212 \pm 0.019$  |
| $a_0$                 | $0.14 \pm 0.06$    | $0.19 \pm 0.06$    | $0.38 \pm 0.06$    |
| $\chi^2/\text{ndf}$   | 23.7/14            | 14.2/11            | 13.7/14            |

to unity at the maximum of the  $\phi$  resonance, is equal to 1.16 at  $E = 1000$  MeV and 0.92 at  $E = 1100$  MeV. The fourth column of Table V presents the parameters obtained taking into account FSI. This model describes all the data on the cross section well. From the difference in  $\chi^2$  between the VMD(18) and VMD+FSI(18) models, we conclude that the significance of the FSI observation in the process  $e^+e^- \rightarrow K_S K_L$  near its threshold is 3.2 $\sigma$ .

The results of the fit in the VMD+FSI(18) model are used to calculate the radiative correction and the energy spread correction. After that, the value of the Born cross section for the process  $e^+e^- \rightarrow K_S K_L$  at the energy point  $i$  is determined as

$$\sigma_i = \frac{N_{K_S K_L, i}}{\varepsilon_i I L_i (1 + \delta_i)(1 + \delta_{E, i})}, \quad (10)$$

The measured energy dependence of the Born cross section is shown in Fig. 10. The fitted curves in the VMD(18) and VMD+FSI(18) models are also presented. The difference between the models is visible in Fig. 10 (left), where the region near the  $e^+e^- \rightarrow K_S K_L$  threshold is shown. This difference is even better visible in Fig. 11 (left), where the ratio of  $\sigma_i$  to the cross-section value at the  $i$ -th point in the VMD+FSI(18) model is shown. The dotted curve shows the ratio of the cross sections in the VMD(18) and VMD+FSI(18) models.

The values of  $(1 + \delta_i)$ ,  $(1 + \delta_{E, i})$  and the cross sections with statistical and systematic errors are listed in Table IV. The main contributions to the systematic uncertainty in the cross section comes from the uncertainties in the luminosity measurement ( $\sim 0.6\%$ ) and the correction calculated in Sec. VII (0.7%). The uncertainties associated with the background subtraction, radiative correction and correction for energy spread are also taken into account. The latter is due to the uncertainty in the measurement of  $\sigma_E$ . It is 0.13% at the resonance maximum. The error in the radiative correction is determined by varying the model parameters within their errors. It changes from 0.01% at  $E = 1000$  MeV to about 0.1% at the resonance maximum and then to 2.8% at  $E = 1100$  MeV. At the resonance maximum, the cross-section accuracy is dominated by a systematic uncertainty, which is about 0.9%.

A comparison of our results with previous measurements is presented in Figs. 11 and 12, which plot the ra-

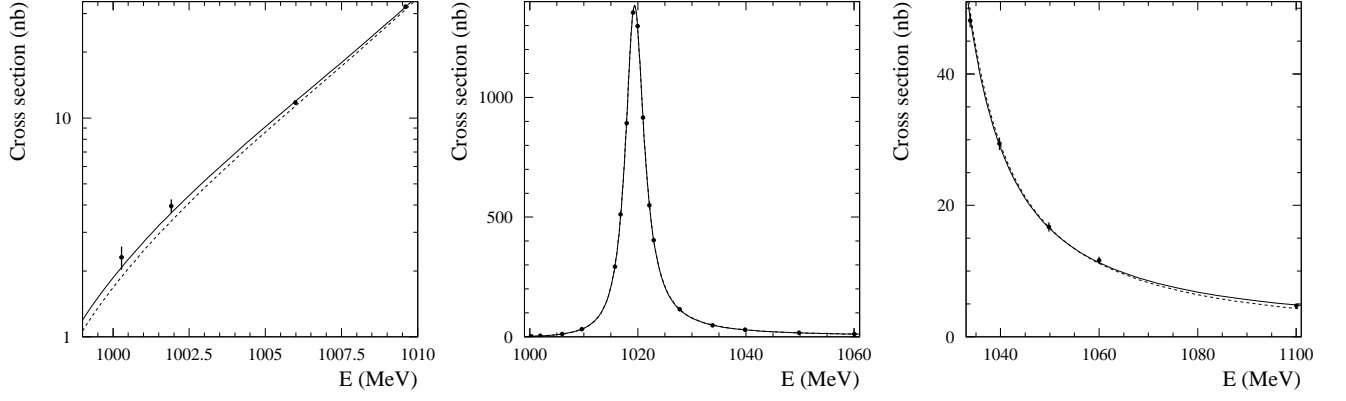


FIG. 10. The measured Born cross section for the process  $e^+e^- \rightarrow K_S K_L$ . The dashed curve is the result of the fit with the VMD(18) model. The solid curve represents the VMD+FSI(18) model.

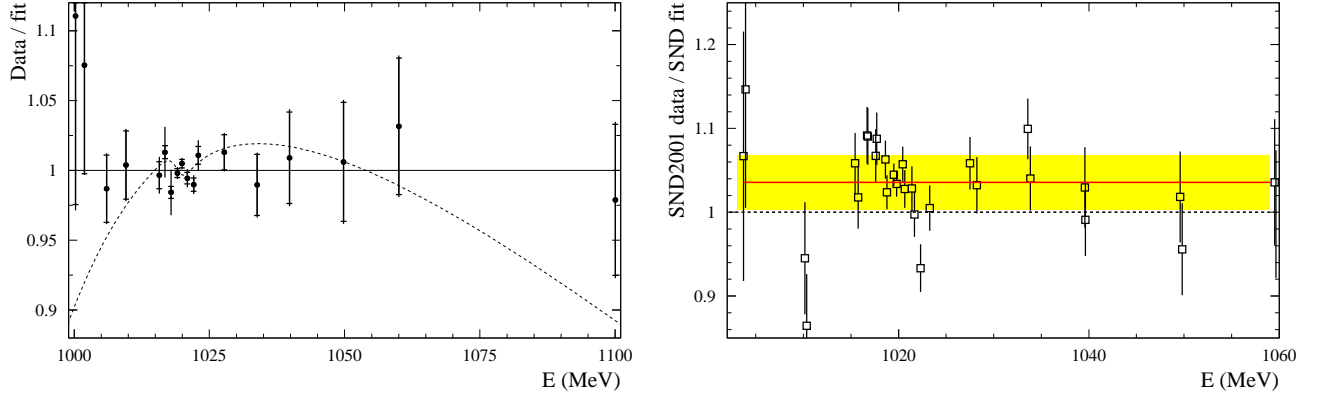


FIG. 11. Left panel: The ratio of the cross section measured in this work to the cross section obtained by fitting with the VMD+FSI(18) model. The dashed curve shows the ratio of the cross sections in the VMD(18) and VMD+FSI(18) models. For the data points, the error bars represent the uncertainties taking into account the inaccuracy of the collider energy setting [see Eq. (7)], with a tick representing the statistical error only. Right panel: The ratio of the cross section measured in the SND experiment at VEPP-2M [5] to the cross section obtained by fitting the data from this work with the VMD+FSI(18) model. The solid line represents the result of the fit to the data with a constant. The shaded box shows the systematic uncertainty of the SND data.

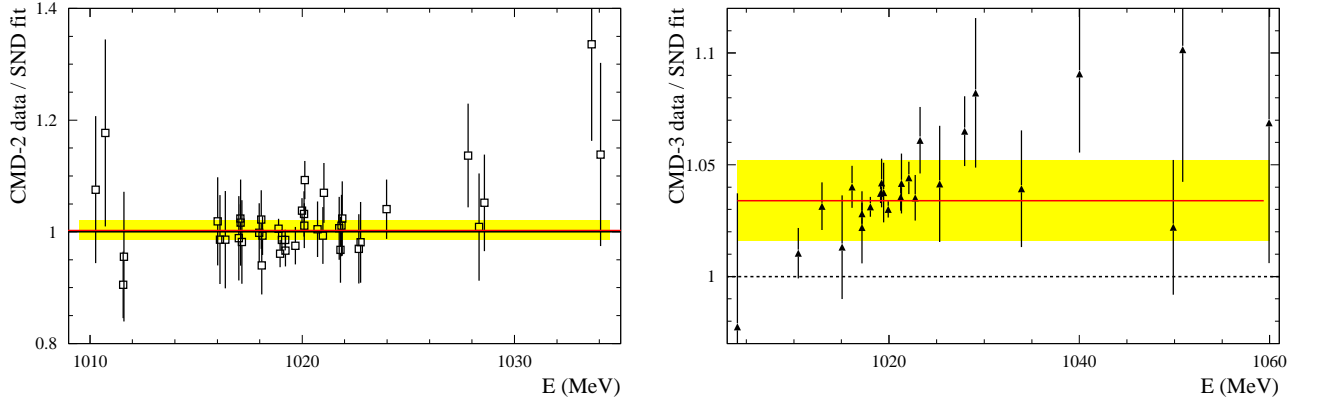


FIG. 12. The ratios of the cross sections measured in the CMD-2 [6] (left) and CMD-3 [1] (right) experiments to the cross section obtained by fitting the data from this work with the VMD+FSI(18) model. The solid line represents the result of the fit to the data with a constant. The shaded box shows the systematic uncertainty of the data.

tios of the cross sections measured in Refs. [1, 5, 6] to the cross section obtained by fitting the data from this work in the VMD+FSI(18) model. The solid line shows the fit of the ratio energy dependence dependence by a constant. The ratio of the SND measurement at VEPP-2M to the new measurement is  $1.036 \pm 0.005 \pm 0.032$ . The same ratios for CMD-2 and CMD-3 are  $1.003 \pm 0.006 \pm 0.017$  and  $1.034 \pm 0.002 \pm 0.018$ , respectively, where the first error is statistical and the second is systematic. The measurements of SND and CMD-2 at VEPP-2M agree with our measurement within the systematic errors. The difference with the CMD-3 measurement is 1.7 standard deviations.

The VMD(15) model is used to obtain the  $\phi$ -meson parameters. Similar models were used to fit the cross-section data in Refs. [1, 5, 6]. As a result of the fit to the measured cross section, the following values of the  $\phi$ -meson parameters are obtained:

$$\begin{aligned} P_\phi &= (9.85 \pm 0.03 \pm 0.10) \times 10^{-5}, \\ M_\phi &= 1019.443 \pm 0.010 \pm 0.060 \text{ MeV}, \\ \Gamma_\phi &= 4.212 \pm 0.20 \pm 0.13 \text{ MeV}, \end{aligned} \quad (11)$$

where  $P_\phi = B(\phi \rightarrow e^+e^-)B(\phi \rightarrow K_S K_L)$ . The first of the quoted errors are statistical, the second are systematic. To determine the systematic uncertainties, we shift all  $IL_i$  or  $\sigma_{E,i}$  up and down by the value of the systematic error. The correction  $a_{\text{cor}}$  is varied within its uncertainty,  $\pm 0.7\%$ . The difference between the interference phase  $\varphi_\phi$  and the quark model prediction ( $180^\circ$ ) can also lead to a change in the parameters. To estimate the magnitude of the possible phase deviation, we use the result  $\varphi_\phi = (163 \pm 7)^\circ$  obtained in Ref. [20] for the  $e^+e^- \rightarrow \pi^+\pi^-\pi^0$  process. To study the systematic uncertainties, we vary  $\varphi_\phi$  from  $180^\circ$  to  $155^\circ$ . The phase of the amplitude  $A_0$  is also changed by  $\pm 25^\circ$ . The parameter  $k_{\text{SU}3}$  is varied from 0.9 to 1.1. The systematic uncertainty of the product  $B(\phi \rightarrow e^+e^-)B(\phi \rightarrow K_S K_L)$  is dominated by the systematic uncertainties in the luminosity and  $a_{\text{cor}}$ . The uncertainty in the mass measurement  $M_\phi$  is completely determined by the systematic uncertainty in the collider energy measurement. The main

source of the systematic uncertainty in  $\Gamma_\phi$  is the uncertainty in the energy spread measurement.

The measured values of the  $\phi$ -meson mass and width are consistent with the PDG values [19], but are less accurate. The PDG value of the product  $B(\phi \rightarrow e^+e^-)B(\phi \rightarrow K_S K_L) = (10.11 \pm 0.12) \times 10^{-5}$  [19] is higher than our measurement by  $1.6\sigma$ .

The uncertainty of PDG  $\phi$ -meson mass  $1019.461 \pm 0.016$  MeV [19] is significantly smaller than the systematic uncertainty of the collider energy measurement (60 keV). Therefore, the PDG mass can be used for calibration of the c.m. energy scale. To do this we introduce into the fit an additional parameter  $\Delta_E$  (common shift of all energy points). Its fitted value

$$\Delta_E = 0.017 \pm 0.018 \text{ MeV} \quad (12)$$

can be used to correct the energies in the first column of Table IV.

## IX. SUMMARY

In the SND experiment at the VEPP-2000 collider, the most accurate measurement of the  $e^+e^- \rightarrow K_S K_L$  cross section has been performed in the center-of-mass energy range from 1000 to 1100 MeV. The systematic uncertainty of this measurement at the maximum of the  $\phi$  resonance is 0.9%. From the fit to the cross section data with the vector meson dominance model, the most accurate value of the product  $B(\phi \rightarrow e^+e^-)B(\phi \rightarrow K_S K_L) = (9.85 \pm 0.03 \pm 0.10) \times 10^{-5}$  has been obtained, which is lower than the PDG value [19] by  $1.6\sigma$ . The measured  $\phi$  meson mass and width are consistent with the PDG values [19]. The best description of the cross-section data near the  $e^+e^- \rightarrow K_S K_L$  threshold has been obtained with the model taking into account the final state interaction. The significance of the FSI effect in our data is  $3.2\sigma$ .

## X. ACKNOWLEDGMENTS

This work was supported by the Russian Science Foundation Grant No. 24-22-0203.

- 
- [1] E. A. Kozyrev *et al.* (CMD-3 Collaboration), Phys. Lett. B **760**, 314 (2016).  
[2] S. G. Sannikov, A. I. Milstein, private communication.  
[3] J. Grange *et al.* (Muon g-2 Collaboration), [arXiv:1501.06858 [physics.ins-det]].  
[4] M. Davier, A. Hoecker, B. Malaescu and Z. Zhang, Eur. Phys. J. C **77**, 827 (2017).  
[5] M. N. Achasov *et al.* (SND Collaboration), Phys. Rev. D **63**, 072002 (2001)  
[6] R. R. Akhmetshin *et al.* (CMD-2 Collaboration), Phys. Lett. B **695**, 412 (2011)  
[7] P. Y. Shatunov *et al.* Phys. Part. Nucl. Lett. **13**, 995 (2016).  
[8] M. N. Achasov *et al.*, Nucl. Instrum. Meth. A **449**, 125 (2000).  
[9] V. M. Aulchenko *et al.*, Nucl. Instrum. Meth. A **598**, 102 (2009).  
[10] A. Y. Barnyakov *et al.*, Nucl. Instrum. Meth. A **598**, 163 (2009).  
[11] V. M. Aulchenko *et al.*, Nucl. Instrum. Meth. A **598**, 340 (2009).

- [12] E. V. Abakumova *et al.*, Nucl. Instrum. Meth. A **744**, 35 (2014).
- [13] E. A. Kuraev and V. S. Fadin, Sov. J. Nucl. Phys. **41**, 466 (1985).
- [14] G. Bonneau and F. Martin, Nucl. Phys. B **27**, 381 (1971).
- [15] J. Allison *et al.* (GEANT Collaboration), Nucl. Instr. Meth. A **835**, 186 (2016).
- [16] M. N. Achasov *et al.* (SND Collaboration), Phys. Rev. D **97**, no.3, 032011 (2018)
- [17] G. Balossini *et al.*, Phys. Lett. B **663**, 209 (2008).
- [18] M. N. Achasov *et al.* (SND Collaboration), Phys. Rev. D **94**, 112001 (2016).
- [19] S. Navas *et al.* (Particle Data Group), to be published in Phys. Rev. D **110**, 030001 (2024).
- [20] M. N. Achasov *et al.* (SND Collaboration), Phys. Rev. D **68**, 052006 (2003).